A Novel Pumping Principle for a Total Artificial Heart

T. Bierewirtz,
K. Narayanaswamy,
R. Giuffrida,
T. Rese,
D. Bortis,
D. Zimpfer,
J. W. Kolar,
U. Kertzscher,
M. Granegger

ETH zürich

A Novel Pumping Principle for a Total Artificial Heart

Tim Bierewirtz *and* Krishnaraj Narayanaswamy, Rosario Giuffrida, *Student Member, IEEE*, Tim Rese, Dominik Bortis, *Senior Member, IEEE*, Daniel Zimpfer, Johann Kolar, *Fellow, IEEE,* Ulrich Kertzscher, *and* Marcus Granegger

Abstract—Objective: **Total artificial hearts (TAH) serve as a temporary treatment for severe biventricular heart failure. The limited durability and complication rates of current devices hamper long-term cardiac replacement. The aim of this study was to assess the feasibility of a novel valveless pumping principle for a durable pulsatile TAH (*ShuttlePump*). *Methods:* The pump features a rotating and linearly shuttling piston within a cylindrical housing with two in- and outlets. With a single moving piston, the ShuttlePump delivers pulsatile flow to both systemic and pulmonary circulation. The pump and actuation system were designed iteratively based on analytical and in silico methods, utilizing finite element methods (FEM) and computational fluid dynamics (CFD). Pump characteristics were evaluated experimentally in a mock circulation loop mimicking the cardiovascular system, while hemocompatibility-related parameters were calculated numerically. *Results:* Pump characteristics cover the entire required operating range for a TAH, providing 2.5 – 9 L/min of flow rate against 50 – 160 mmHg arterial pressures at stroke frequencies of 1.5 – 5 Hz while balancing left and right atrial pressures. FEM analysis showed mean overall copper losses of 8.84 W, resulting in a local maximum blood temperature rise of < 2 K. The CFD results of the normalized index of hemolysis were 3.57 mg/100L, and 95% of the** pump's blood volume was exchanged after 1.42 s. *Conclusion and significance:* **This study indicates the feasibility of a novel pumping system for a TAH with numerical and experimental results substantiating further development of the ShuttlePump.**

*Index Terms—***Biventricular heart failure, blood pump, computational fluid dynamics, hemocompatibility, rotary piston pump, total artificial heart.**

I. INTRODUCTION

MECHANICAL circulatory support (MCS) became the therapy of choice for end stage heart failure patients who are not eligible for heart transplantation [1]. Ventricular assist devices (VADs) account for the vast majority of all MCS implantations, with 13025 cases in US from 2014-2018. In contrast, 200 total artificial hearts (TAHs) were implanted in the same era [2]. However, these low numbers of TAH implantation rather reflect the limited availability of devices than the medical need [3].

Emerging patient populations in need of a TAH are patients with severe biventricular failure, cardiac tumors, congenital heart disease, or univentricular physiologies. In all these patients, conventional VADs are either not applicable or lead to worse clinical outcomes in terms of survival than in typical VAD patients with left ventricular failure [4], [5].

The TAH implantation numbers may be limited by complications associated with the intrinsic characteristics of their underlying pumping principle. Clinically used bridge to transplant TAH systems, such as SynCardia TAH (SynCardia systems Inc, Tucson, AZ, USA) and Aeson, The CARMAT TAH (Carmat Vélizy-villacoublay, France) are pneumatical/hydraulically actuated positive displacement pumps. They mimic the native heart function by creating physiological, pulsatile flow utilizing diaphragms and valves. Other positive displacement TAH concepts such as ReinHeart TAH [6] and Realheart TAH [7] feature a comparable pumping principle. In contrast, they directly generate the volume displacement via electro-mechanical actuation without using pneumatics or hydraulics.

The size and technical complexity of these positive displacement pumps may hamper their translation toward a destination therapy [8].

Rotodynamic blood pump (RBP) technology enables the development of small and efficient pump designs. TAH concepts, such as the Cleveland continuous flow TAH [9] and the BiVACOR TAH [10], utilize a single rotating part with back-to-back impeller arrangement to facilitate flow in both systemic and pulmonary circulation. Similarly, the OregonHeart TAH [11] employs a pumping mechanism based on RBP technology. However, the rotating impeller switches

Tim Bierewirtz, Tim Rese, and Ulrich Kertzscher are with the Deutsches Herzzentrum der Charité (DHZC), Institute of Computer-assisted Cardiovascular Medicine, Biofluid Mechanics Laboratory Berlin, 13353 Berlin, Germany *and* with the Berlin Institute of Health at Charité - Universitätsmedizin Berlin, BIH Innovation - Team SPARK, 10178 Berlin, Germany.

Krishnaraj Narayanaswamy is with the Department of Cardiac Surgery at Medical University of Vienna, 1090 Vienna, Austria.

Daniel Zimpfer is with the Department of Cardiac Surgery at Medical University of Vienna, 1090 Vienna, Austria and with the Department of Cardiac Surgery, Medical University of Graz, 8036 Graz, Austria.

Rosario Giuffrida, Dominik Bortis, and Johann Kolar are with the Power Electronic Systems Laboratory, ETH Zürich, 8049 Zurich, Switzerland.

Marcus Granegger is with the Department of Cardiac Surgery, Medical University of Vienna, 1090 Vienna, Austria, and with the Deutsches Herzzentrum der Charité (DHZC), Institute of Computer-assisted Cardiovascular Medicine, Biofluid Mechanics Laboratory Berlin, 13353 Berlin, Germany *and* with the Berlin Institute of Health at Charité - Universitätsmedizin Berlin, BIH Innovation - Team SPARK, 10178 Berlin, Germany (Email: marcus.granegger@meduniwien.ac.at).

the pump output from the systemic to pulmonary circulation by an axially shuttling motion, generating pulsatile flow without the need for pump speed modulations.

The low complexity of the TAH concepts based on RBP technology might be advantageous over displacement pumps in terms of durability and size. However, this pumping principle is associated with high shear rates, suspected to induce hemocompatibility-related adverse events such as gastrointestinal bleeding and thromboembolic complications [12].

Rotary piston pumps offer an alternative pumping principle that may have the potential to overcome limitations of current technologies: They may be smaller, more durable (no membrane and valves), more efficient than pulsatile devices, and concomitantly provide pulsatile flow with a potentially less traumatic pumping principle than RBPs. However, their actuation and bearing concepts are usually complex [13]. Theoretical derivations suggest that if reliable drives and bearings are developed for these pump technology, rotary piston blood pumps may become a promising alternative [13].

The first innovative blood pump concepts inspired by rotary piston pumps indicated the technical feasibility and the preclinical potential of such approaches [14], [15]. Yet, none of these devices has been translated into the clinical arena.

The aim of this study was to investigate a novel TAH (the *"ShuttlePump"*) based on an innovative pumping concept, which may potentially combine the advantages of both pulsatile and RBPs– by delivering pulsatile flow with less blood trauma and low technical complexity with a minimum number of moving parts.

II. Materials and Methods

A. Clinical Requirements and Device Design

1) Mechanical Design and Vascular Connection

Requirements for implantable TAHs regarding the mechanical design include (i) similar spatial dimensions as the native ventricles for implantability, (ii) high durability for use as a long-term therapy, (iii) the use of hemocompatible materials in blood contact, (iv) versatile anatomically oriented vascular connections to permit implantation in a large patient population.

These requirements were considered in the initial design of the proposed TAH concept: The pump features a cylindric piston (Ø48.72 mm; L = 68 mm) with two opposite notches that divide the cylindric pump housing (ID = Ø49 mm; L = 100 mm) into two chambers, depicting the left and right ventricular chambers. Both chambers are connected to one in- and outlet each. Medical grade titanium ducts at the in- and outlets are connected to soft vascular grafts intended to be anastomosed to the atria and large arteries, respectively.

The blood-leading parts of the pump housing are fabricated of silicon carbide as it features high thermal conductivity and good hemocompatibility [16]. The outer shell of the piston is made of polyether ether ketone (PEEK) because of its hemocompatibility [17].
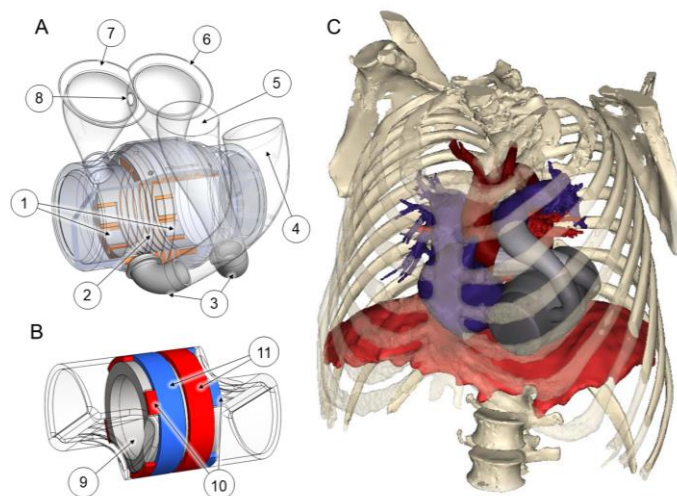

Fig. 1. A. Cutaway view of the pump housing with the rotary motor stator (1) and linear motor stator (2), titanium outflow connectors (3), soft vascular grafts towards aorta (4), pulmonary artery (5), right atrium (6), left atrium (7) and orifice as interatrial shunt (8), B. Piston with inner back iron (9), rotary (10) and linear (11) permanent magnets, C. Virtual pump implantation in an adult male patient with BSA of 1.89 m^2 (ethics approval obtained at the Medical University of Vienna (EK-Nr: 1856/2021))

2) Hydraulic Design

The requirements of TAHs in terms of hydraulic performance include (i) the delivery of sufficient and pulsatile blood flow (2.5 - 9 L/min) in both systemic and pulmonary circulation against systemic arterial pressures of up to 160 mmHg, (ii) low blood trauma and thrombogenic potential and (iii) the achievement of flow balance between the left and right pump output to avoid pulmonary congestion.

The pump is designed to displace a volume of 30.2 ml per stroke to achieve the required hydraulic performance. Adjusting the shuttling frequency from 1.5 to 5 Hz may reach cardiac outputs from 2.5 to 9 L/min. The piston is actuated in a continuous rotary and synchronized linear shuttling motion with a saturated sinusoidal motion profile with 16 mm of amplitude (Fig. 2). The linear motion fills one chamber while discharging the other chamber simultaneously. The rotary motion ensures an overlap of the piston notches with the in- or outlets of the chambers. This way, the rotary motion coordinates the filling and discharging of both chambers without the need for mechanical check valves and with only one rigid moving part. The rotation of the piston causes the fluid film inside the micro gap to act as a hydrodynamic bearing and stabilize the piston to avoid contact with the housing during pump operation. A contactless piston motion is essential to avert wear, blood damage, and thrombus initiation.

In the native heart, the cardiac output of the left ventricle exceeds the one on the right side because of the bronchial shunt flow. Since only a single moving part is utilized in the proposed concept, the pump output of both sides is not independently adjustable, bearing the risk of pulmonary congestion [18]. Therefore, the left-right balance is intended to be achieved by an inter-atrial shunt by penetrating the remaining atrial septum of the patient or the atrial vascular connections (Fig. 1. A. 8).
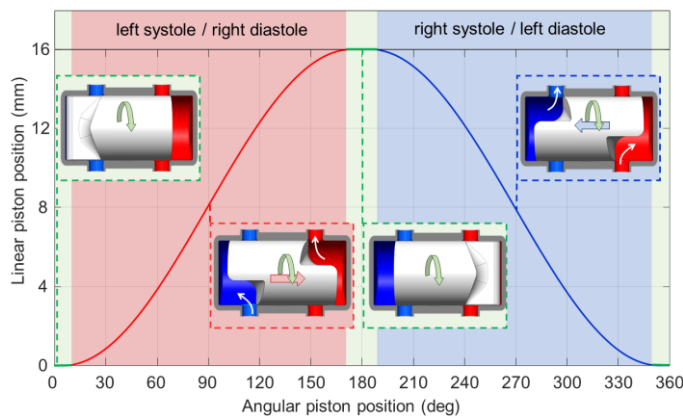
Fig. 2. Linear piston position (in mm) over angular piston position (in degree) for one pump cycle with a schematic depiction of pumping principle at four positions. At 0 and 180 degrees, the piston closes both in- and outlets, so linear motion is disabled to avoid pressure peaks (green). After 5 degrees of rotation, the left systole/right diastole (red) starts with the linear piston motion profile from the right (0 mm) to the left side (16mm), synchronized to continuous rotation, followed by sole rotation between 175 and 185 degrees (green). Right systole/left diastole starts after 185 degrees (blue).

3) Actuation Design

Requirements for the electromagnetic actuation of the ShuttlePump include (i) sufficient force and torque generation for pump operation, (ii) limited motor heat losses to prevent the increase in local blood temperature above 2 K [19], (iii) low power consumption for long battery lifetime and the potential for transcutaneous energy transfer (TET).

For this, a linear-rotary actuation system was designed using methods and topologies presented by Giuffrida et al. [20] with respect to the geometric limitations of the pump system. A set of permanent magnets placed on a back iron are incorporated inside the piston (Fig. 1. B.), forming two opposite radially magnetized rings in the central part for linear force generation and four poles beside for rotational motion. A stator is placed between the in- and outlet region of the pump housing (Fig. 1. A.) with 6 ring copper coils in a 3-phase configuration in the central part and 6 semi-closed slots on each side for torque generation.

B. Evaluation of Hydraulic Characteristics and Hemocompatibility Related Parameters

To evaluate the hydraulic characteristics and hemocompatibility of the proposed TAH, we followed a systematic approach by utilizing analytical, in silico, and in vitro methods (Fig. 3)
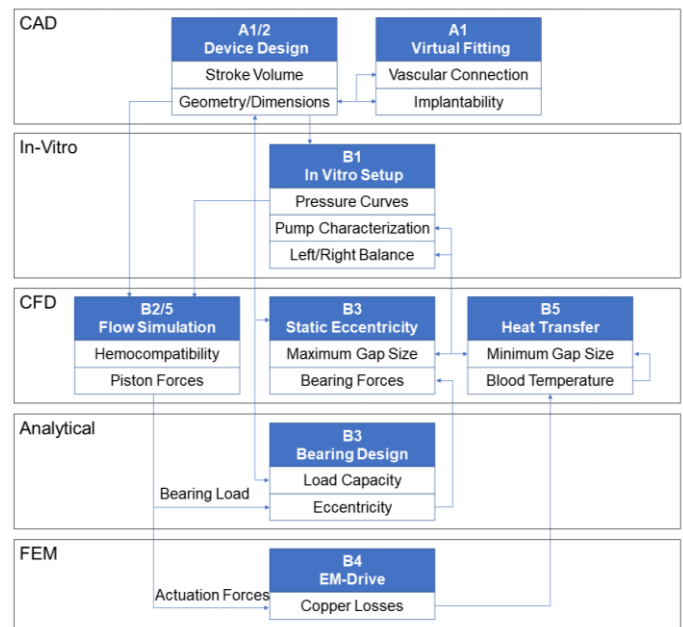

Fig. 3. Flow chart of methods used for iterative pump design and evaluation, initiated from the top left box. The blue boxes represent the referent chapters, and the white boxes indicate the results obtained from the specific chapter, and the arrows show results that were used as inputs for the following methods. Basic methods from top to down: CAD (Computer Aided Design), in vitro, CFD (Computational Fluid Dynamics), Analytical, FEM (Finite Element Method).

1) In Vitro Hydraulic Characterization

To assess the hydraulic pumping performance, a functional pump system was manufactured from a borosilicate precision glass cylinder (ID = Ø50 mm; L = 105 mm) with drill holes (D = Ø11mm) at the in- and outlet positions. 3D-Printed polymer caps at the sides, tube connectors, and two stiff chambers representing artificial atrial chambers were tightly mounted onto the glass. A PEEK piston was thermally bonded onto a stainless-steel shaft (D = Ø10 mm) and precisely milled with a 140 µm micro-gap clearance with respect to the glass. The gap clearance was chosen based on the preliminary analytical and CFD results (Section II B3 and II B5). The shaft ends protrude out of both caps through radial shaft seals (RWDR 72 NBR 902, 10x18x6, Freudenberg, Weinheim, Germany), allowing an external actuation of the piston by connecting one shaft end via a shaft coupling (Loewe GK27, Schmidt-Kupplung GmbH, Wolfenbüttel, Germany) to a linear-rotary motor (PR01-52x40-R/37x120F-HP-C-80, NTI AG, LinMot & MagSpring, Spreitenbach, Switzerland). To compensate for the reduction in effective stroke volume by the protruding shaft ends, the piston's diameter is slightly increased compared to the model used for in silico studies (50 mm vs. 49 mm), resulting in comparable stroke volumes for comparable pump characteristics. The rotary frequency was set to the desired pump rate, while the linear shuttling motion followed the motion profile depicted in Fig. 2.

A mock circulatory loop was developed and connected to the hydraulic model (Fig. 4). The test bench consists of 2 serial circuits mimicking the pulmonary and systemic circulation, consisting of reservoirs, silicon tubing ($^3/_8$ in and ½ in), and hydraulic resistances. Open reservoirs with volumes of 5 and 1

litre, mimicked the systemic and pulmonary venous systems, respectively. Air-trapped reservoirs (3 litre air in pulmonary artery PA, 1 litre in aorta Ao) in combination with hydraulic resistances (pulmonary resistance PR and systemic resistance SR) were adjusted to achieve realistic pulmonary and systemic arterial Windkessel properties, respectively. A shunt tube with an adjustable clamp was connected between the aortic and pulmonary vein pathways to account for the bronchial circulation.
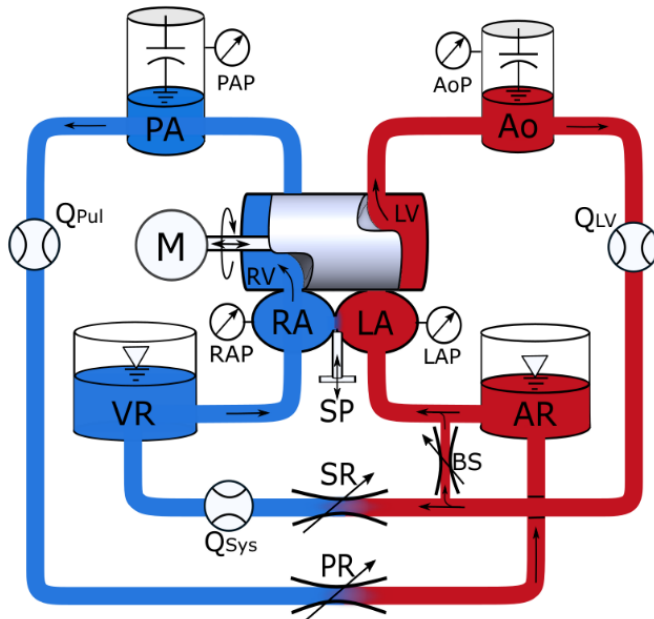

Fig. 4. Schematic mock loop connected to the hydraulic pump model driven by an external motor (M). Blue: pulmonary circulation with venous reservoir (VR), right atrium (RA) with a pressure sensor to measure the right atrial pressure (RAP), right ventricle (RV), pulmonary artery (PA) as an air-trapped reservoir with a pulmonary artery pressure (PAP) sensor, pulmonary flow sensor (Q_{Pul}) and adjustable clamp for pulmonary resistance (PR). Red: systemic circulation with arterial reservoir (AR), left atrium (LA) left atrial pressure (LAP) sensor, left ventricle (LV), aorta (Ao) with an air trapped reservoir with an aortic pressure (AoP) sensor, left ventricular flow sensor (Q_{LV}), bronchial shunt with adjustable clamp (BS), adjustable clamp for systemic resistance (SR) and systemic flow sensor (Q_{Sys}). Different shunt diameters can be set between RA and LA via a shunt plug (SP).

Arterial pressures were measured at the air-trapped reservoirs and atrial pressures at the artificial atria with APT300 pressure sensors (Harvard Apparatus, Holliston, MA, USA). Flows were recorded at both tubes connecting the arterial with the venous reservoirs and before the bronchial shunt utilizing ultrasonic clamp-on sensors (SONOFLOW CO.55, Sonotec, Halle, Germany). Signals were acquired at 1 kHz (DS1104, dSpace, Paderborn, Germany). All experiments were performed with blood-mimicking fluid (water-glycerol-mixture 60/40 %v/v, T = 20 °C).

Plugs with orifices of different diameters (0 mm, 4 mm, 6 mm, 8 mm, 10 mm) were incorporated between the left and right atrium, acting as interatrial shunts of different diameters. The difference between the mean left and right atrial pressure (dAP = mLAP - mRAP) was recorded over time after changing from 10 mm to 8 mm, 6 mm, 4 mm, and 0 mm, respectively. A low and stable dAP over time indicates an adequate left-right balance to avoid pulmonary congestion.

As a typical operating condition for a TAH, hydraulic resistances (SR and PR) were adjusted to meet a mean arterial pressure of 90 mmHg and a mean pulmonary arterial pressure of 25 mmHg under a mean systemic flow rate (mQ_{Sys}) of 4.5 L/min. The bronchial shunt resistance (BSR) was set to achieve a mean bronchial shunt flow (mQ_{BS}) to mean systemic flow (mQ_{Sys}) ratio of 1:10.

For a pump characterization in terms of pressure and flow properties over the entire physiological range, five different systemic resistances (SR) and pump frequencies from 1.5 Hz to 4.5 Hz were investigated where the mean bronchial shunt flow mQ_{BS} was always adjusted to 10% of the mean systemic flow.

2) In Silico Hydraulic Characterization and Force Prediction

The numerical assessment of the flow field and hemocompatibility of the ShuttlePump was performed utilizing CFD in Star-CCM+ solver (Siemens, Munich, Germany). An overset mesh methodology was employed to realize the piston's motion. A high-quality mesh with 5.7 million hexahedral elements (after initialization of overset interface) with four prism layers in the hydrodynamic bearing gap region was set up to accurately capture the flow behavior. The mesh quality metrics were carefully evaluated throughout the simulation to comply with the guidelines specified in the solver's user manual [21]. The average Y+ value was 0.6 to resolve the viscous sublayer and to model the near-wall turbulence. Furthermore, 99.999% of the surfaces were found to lie within the viscous sublayer.

Parameters such as average wall shear stress on housing and piston, force and torque acting on the piston, and volume of blood exposed to shear >9 Pa were evaluated for the mesh convergence study. Three different mesh sizes were utilized (3.7 million, 5.7 million and 14.8 million). The maximum relative error between the 5.7 million and 14.8 million meshes was below 5%. Consequently, the mesh size of 5.7 million was chosen for subsequent evaluations. Further details on the mesh were elaborated in Supplementary 2.

The properties of the operating fluid were considered Newtonian with a constant density of 1050 kg/m^3 and dynamic viscosity of 3.5 mPas [22]. An unsteady Reynolds averaged Navier-Stokes simulation (URANS) was performed by modeling the turbulence using Menter's K-ω shear stress transport model [23]. The simulation was performed for every 1-degree rotation of the piston. A 3 Hz rotational frequency combined with a modified sinusoidal translational motion was specified for the piston motion (Fig. 2) (Supplementary Video 1). The boundary conditions for in- and outlets were the time-resolved pressure curves over one piston cycle, recorded from the in vitro setup (Section B1). All other boundary regions were defined as wall boundaries with no slip.

3) Analytical and In Silico Bearing Load Capacity Considerations

A hydrodynamic bearing (HB) has been designed to levitate the piston without mechanical contact with the pump housing for a reliable and hemocompatible pump operation. For this purpose, the HB design needs to account for the piston's weight and the hydrodynamic load acting on the piston.

Further, the electromagnetic drive unit, i.e., the linear and rotary motor, will be placed in the region of the HB. The copper losses of the motor coils constitute a heat source; hence the bearing design needs precise consideration to distribute the heat. Based on preliminary analytical load capacity calculations and numerical evaluations of thermal distribution, a gap clearance of 140 μm was initially chosen (Supplementary 1).

In general, analytical approaches to predict the load capacity of HBs are valid for short or long cylindrical bearings with rotational motion [22], [24]. However, in the ShuttlePump, the geometry of the piston with its notches renders a purely analytical approach difficult.

To account for the influence of these side notches on the load capacity, the effective length (l) of the hydrodynamic bearing over time was characterized. For this purpose, we numerically computed the hydraulic forces using CFD for four different static eccentric positions (eccentricity ratio ε – 0.2, 0.4, 0.6, 0.7), considering only the rotational motion (3 Hz) of the piston.

The relatively small bearing gap resulting from the different eccentric positions of the piston necessitated hexahedral mesh elements of 3.9, 23.7, 23.6 and 23.9 million for eccentricities 0.2, 0.4, 0.6 and 0.7, respectively. To facilitate the rotational motion, a sliding mesh approach was employed. Mesh convergence study was performed with three different mesh sizes for four different eccentric positions, the maximum relative error in hydraulic forces were less than 6% for the medium mesh utilized for this study. The details regarding the meshing strategy and mesh convergence study can be found in Supplementary 1. The fluid properties and the implementation for the numerical simulation were the same as described in Section B2. The piston and housing were modelled with a no-slip wall boundary condition. The in- and outlets were set to a zero gradient pressure boundary.

In the next step, based on the simulation results, the effective length (l) of the bearing was identified by fitting l with a nonlinear least square approach to solve equation 1 [22].

$$\text{W} = \frac{\mu \omega R l^3}{2c^2} \quad \frac{\pi}{2} \quad \frac{\varepsilon}{(1-\varepsilon^2)^{3/2}} \qquad (1)$$

Where W is the load in N, ω is the angular velocity in rad/s, μ is the dynamic viscosity of the fluid in Pa-s, c is the gap clearance between piston and housing in m, ε is the eccentricity ratio ($\varepsilon = {}^e/_c$, e – eccentric position in m), R is the mean bearing radius in m, and l is the effective length of the bearing in m.

Using this effective bearing length, the load capacity was analytically extrapolated for eccentricity ratios varying from 0 to 1.

4) In Silico Electric Power Consumption Prediction

Based on the predicted axial force and torque acting on the piston, we used FEM simulations of the electromagnetic drive to predict the instantaneous copper losses during one pump cycle. The 3D FEM model includes the full geometry of the linear-rotary actuator, consisting of the cores and windings of the linear and rotary stators and the permanent magnets of the mover embedded in the piston. The mesh quality for the FEM simulations is guaranteed by the solver of the utilized software (ANSYS Maxwell). With an iterative approach, the mesh is

refined until specific energy-balance convergence criteria are satisfied, with an energy error threshold as low as 1% [25].

The instantaneous ohmic losses are predicted as follows: From the results of the FEM simulations, it is possible to obtain a force constant $k_{F,FEM}$ for the linear actuator and a torque constant $k_{M,FEM}$ for the rotary actuator for every position in the motion profile of Fig.2. Their values relate the generated force and torque proportionally to the amplitude of the force- and torque- generating currents (using Field-Oriented Control) impressed in the corresponding stator windings. Therefore, with the predicted axial force and torque profiles $f_{req}(t)$ and $m_{req}(t)$, the required force and torque generating currents ($i_{lin}(t)$ and $i_{rot}(t)$) versus time are,

$$i_{lin}(t) = \frac{f_{req}(t)}{k_{F,FEM}(t)} \text{ and } i_{rot}(t) = \frac{m_{req}(t)}{k_{M,FEM}(t)} \qquad (2)$$

From the results of the FEM simulations, also the resistance of the coils of the linear and rotary stators $R_{c,lin}$ and $R_{c,rot}$ are obtained and used to predict the instantaneous ohmic losses ($p_{Cu}(t)$) as:

$$p_{Cu}(t) = p_{Cu,lin}(t) + p_{Cu,rot}(t)$$
$$= R_{c,lin} \cdot i_{lin}^2(t) + R_{c,rot} \cdot i_{rot}^2(t) \qquad (3)$$

5) In Silico Hemocompatibility Prediction

For hemocompatibility predictions, the traumatic and thrombogenic potential of the ShuttlePump was analyzed regarding blood damage [26], local blood temperature rise, and pump washout [27]. Blood trauma was numerically quantified by computing the normalized index of hemolysis (NIH) using the power law model with constants of Giersiepen *et al*. [28]. The implementation of the power law model in the computational domain followed the procedures described by Garon and Farinas [26] (Supplementary 3). A passive scalar transport equation was implemented at the inlets to analyze the washout behavior of the pump.

Further, a conjugative heat transfer (CHT) simulation was performed with silicon carbide material properties and a housing shell thickness of 0.5 mm to analyze the thermal distribution across the fluid domain. The solid domain was discretized with 5.45 million hexahedral mesh elements. To quantify the variation in temperature, the thermal properties of the blood thermal conductivity (0.5 W/m/K) and specific heat (3650 J/kg/K) [29] were additionally specified. The overall copper losses for the linear and rotary motors (Section B4) were imposed along the outer circumference of the housing shell as a heat source to analyze the local blood temperature increase evoked by motor coil heat losses.

III. RESULTS

1) In Vitro Hydraulic Characterization

Hemodynamics of the typical operating condition over three pump cycles at 3 Hz and an interatrial shunt with D = 8 mm are depicted in Fig. 5. For a mean arterial pressure (MAP) of 90 mmHg, we observed a diastolic arterial pressure of 79 mmHg

and a systolic arterial pressure of 102 mmHg. The PAP alternates between 20 mmHg and 29 mmHg around a mean value of 25 mmHg. The LAP oscillates between 35 mmHg and -12 mmHg, with a mean value of 11 mmHg. RAP reaches values from -16 mmHg to 33 mmHg, with a mean pressure of 6 mmHg. The output flow of the left ventricle ($mQ_{LV} = 5$ L/min) was lower than on the right side ($mQ_{Pul} = 5.17$ L/min), reflecting a mean gap flow mQ_{GAP} from the left to the right chamber of about 0.17 L/min. The difference of 0.5 L/min between mQ_{LV} and mQ_{Sys} represents the mean bronchial shunt flow mQ_{BS}.
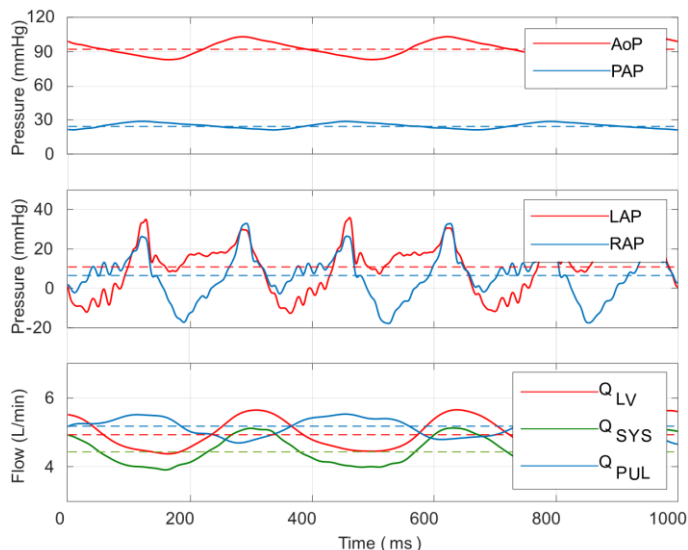

Fig. 5. Recorded pressures and flows at 3Hz for a typical pump operation point and IAS of 8mm diameter. Top: Aortic pressure (AoP) and pulmonary artery pressure (PAP). Middle: Left atrial pressure (LAP) and right atrial pressure (RAP). Bottom: Left ventricular flow (Q_{LV}), Systemic Flow (Q_{SYS}), and pulmonary flow (Q_{PUL}). The dashed lines correspond to the mean values.

The hydraulic pump characteristics are presented in Fig. 6 in terms of the MAP over the mean systemic flows for different resistance scenarios, with pumping frequencies rising from 1.5 Hz to 4.5 Hz.
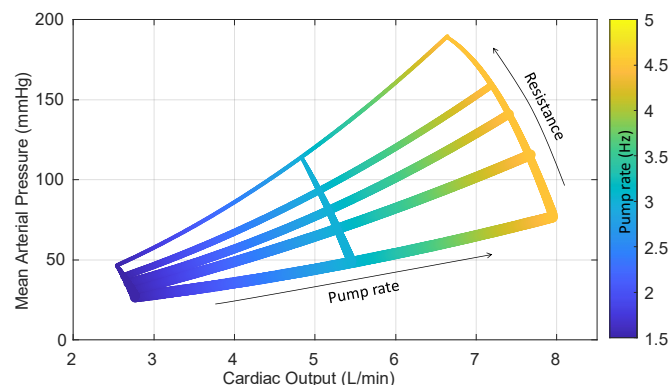

Fig. 6 MAP over the cardiac output for different pump rates (color bar) and resistance setting, where the width of the curves corresponds to the adjusted resistance applied.
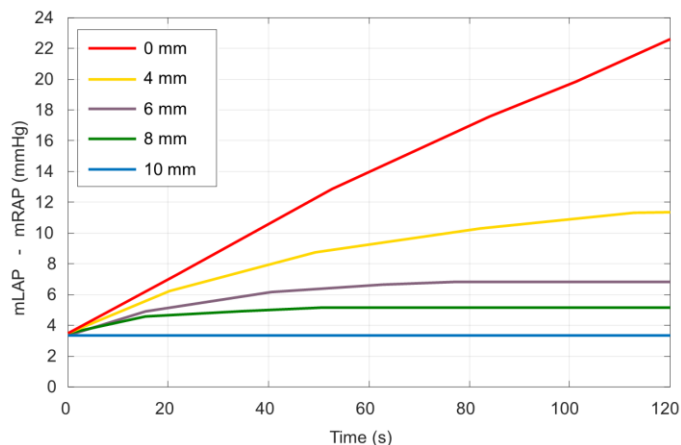

Fig. 7. Difference between mean left atrial pressure (mLAP) and mean right atrial pressure (mRAP) over time for different interatrial shunt diameters.

The efficacy of the interatrial shunt to achieve a left-right balance with different diameters is depicted in terms of the difference between mLAP and mRAP over a period of 120 s (Fig. 7). For D = 10 mm, a constant mean difference of 3.5 mmHg was measured. 8- and 6-mm diameters caused a stable difference of 5.5 mmHg and 7 mmHg after 50 s and 75 s, respectively. With D = 4 mm, the pressures were still changing after 120 s with a final difference of 11.5 mmHg. A closed interatrial shunt (D = 0 mm) led to a steady increase in pressure difference and finally caused an overflow of the pulmonary venous reservoir, reflecting pulmonary congestion.

2) In Silico Hydraulic Characterization and Force Prediction

The numerical results predicted a mean volume flow rate of 4.86 L/min and 5.48 L/min achieved over one pump cycle in the systemic (Q_{Sys}) and pulmonary (Q_{Pul}) circulation, respectively. The bearing gap of 140 μm was well resolved in the CFD simulations, with a net flow from the left chamber (systemic) to the right chamber (pulmonary) of 0.12 L/min. The flow field at four different angular positions is visualized in Fig. 8. Unstructured eddies were observed in the pump chambers during the cycle with an average velocity of < 3 m/s.
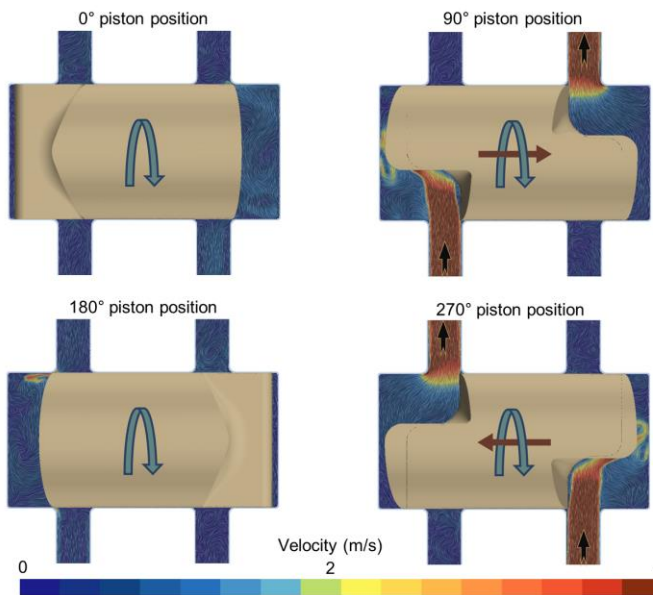
Fig. 8. Visualization of the flow field at different angular position of the piston. A non-uniform low-velocity flow was observed in the chambers. 0° indicates closed in-/outlets with piston on left extreme position, 90˚ - completely open pulmonary inlet and systemic outlet, 180˚ - closed in-/outlets with piston on right extreme position, and 270˚ - completely open pulmonary outlet and systemic inlet.

Hydraulic forces acting on the piston are depicted in Fig. 9, with a maximum axial force of 49.2 N and a mean radial force of 18.7 N. The mean rotational torque in the axial direction was 3.1 mN-m. The time-varying hydraulic forces and torque for one pump cycle were utilized as the boundary condition for the design of the electromagnetic actuation system (Section B4).
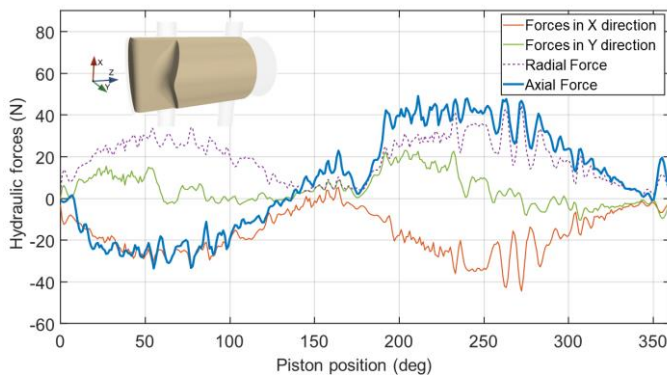

Fig. 9. Hydraulic forces acting on the piston over one pump cycle at 3Hz rotational frequency and for the defined pressure boundary condition.

3) Analytical and In-Silico Bearing Load Capacity Considerations

Fig. 10 shows the numerically predicted mean hydraulic forces for the 140 μm bearing gap in piston geometry with four static eccentric positions and the fitted load capacity curve. Fitting results indicate a mean effective bearing length of 36.7 mm. The presence of piston notches alters the pressure distribution along the circumference over time, leading to an effective bearing length fluctuation during each cycle, with a range between 34.8 and 38.1 mm. The numerically predicted

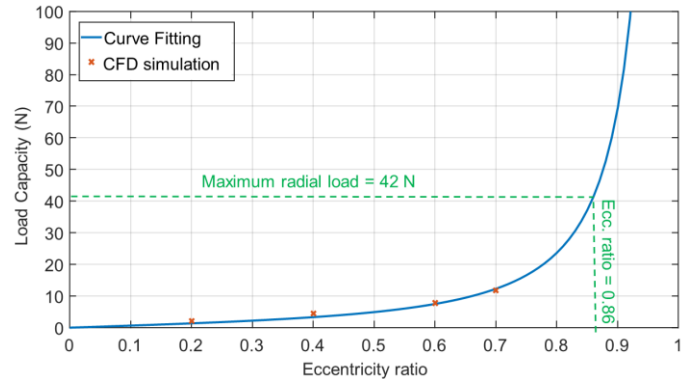hydraulic forces (Section B2) match the bearing load capacity at an eccentricity ratio below 0.86.

Fig. 10. Bearing load carrying capacity plotted against eccentricity ratio for a piston with a 140 μm gap size, along with the corresponding fitted curve. The results indicate a proportional relationship between load capacity and the piston's eccentric position, with the load increasing exponentially as eccentricity increases.

4) In Silico Electric Power Consumption Prediction

The instantaneous ohmic losses of the EM drive were predicted over time, visualized in Fig 11. The power losses of the linear actuator are the dominant component, with the power losses of the rotary actuator only contributing about 70 mW on average to the total average (continuous) power losses of 8.84 W. The peak power losses (about 33.5 W) occur only for a short transient during the left systole when the largest axial force is required.
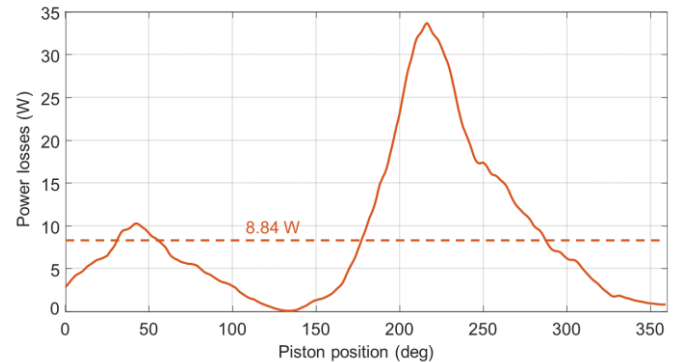
Fig. 11. Predicted total power losses of the linear-rotary actuator over one pump cycle.

5) In Silico Hemocompatibility Prediction

The numerically computed NIH for the ShuttlePump was 3.57 mg/100L. Maximum shear stresses were observed during the opening and closing of the in- and outlets, with a peak magnitude of 107 Pa. Comparatively lower shear stresses were observed within the hydrodynamic bearing gap with a maximum of 82 Pa.

The predicted washout behavior of the pump over eight pump cycles is shown in Fig. 12 (Supplementary Video 2). The time point at 0 seconds represents the blood without dye injection. After the first cycle, 50% of the old blood was replaced. At 1.42 s, 95% of the old blood volume was exchanged. Discrete analysis of washout behavior in planar sections along the linear

Fig. 12. Washout and thermal analysis over eight consecutive pump cycles. The plot shows the washout volume and local blood temperature rise in the ShuttlePump. The left axis represents the percentage of pump washout volume over cycles, while the right axis displays the maximum local blood temperature rise in K. The blue dashes indicate a 95% washout, and the red dashes represent an asymptotic rise in temperature with a maximum of 1.7 K. The top 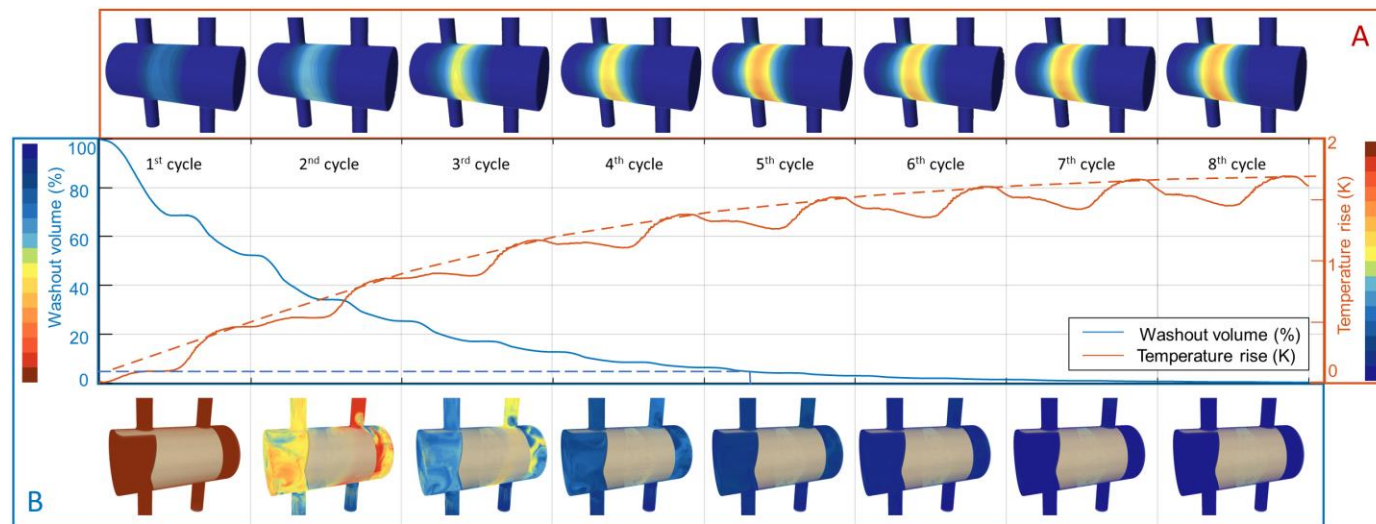image (A) displays the temperature distribution over the circumference of the pump, demonstrating a shift in maximum temperature towards the right chamber. The bottom images (B) depict the pump's washout behaviour, with dark red indicating the old blood concentration before the dye injection and blue representing the new blood.

axis within the HB gap revealed 95% bearing washout in 1.47 s.

The converged CHT simulation indicated a maximum local temperature rise of 1.7 K for the specified mean copper loss of 8.84 W (Fig 12). Due to the pressure difference, fluid flow predominantly occurred from the systemic chamber to the pulmonary chamber within the bearing gap. Consequently, the maximum temperature region shifted towards the pulmonary chamber (Fig 12, A).

IV. DISCUSSION

The unmet medical need for a durable TAH with improved hemocompatibility may be addressed by innovative pumping principles such as rotary piston pumps. However, the complexity of realizing the motion in previously presented piston pumps [8] hinders the clinical translation. In this study, we assessed the technical feasibility and in silico hemocompatibility of a TAH utilizing a novel, less complex rotary piston pump principle. The proposed concept might overcome the drawbacks of current displacement pump concepts by means of low complexity and small size. At the same time, it might be advantageous over RBPs because of lower shear rates.

The spatial dimensions of the ShuttlePump were designed to ensure implantability in adult patients. Preliminary virtual implantations indicate adequate size and geometry to address the intended patient population. The pump's spatial design directly affects its hydraulic performance, the stroke volume of 30.2 ml of the pump chambers determines the required stroke frequency to achieve the desired pump output. The pump covered flow rates from 2.5 to 8 L/min against arterial pressures up to 180 mmHg at frequencies from 1.5 to 4.5 Hz.

In contrast to RBPs [30], the ShuttlePump is less sensitive to pre- and afterload over the entire operating range. Therefore, an automated physiologic control system may be required to adapt the pump output to the need of the patient. However, even with a physiologic control system, the pumping principle of the ShuttlePump does not permit independent adaption of the left and right pump output. Therefore, we introduced an interatrial shunt to balance the atrial pressures and prevent pulmonary congestion, leading to a stable difference between mLAP and mRAP of <7 mmHg at shunt diameters >6 mm. The patency and safety of similar inter-atrial shunts were recently shown in HFpEF (Heart Failure with preserved Ejection Fraction) patients [31], yet these patients were not supported by any MCS systems. Therefore, the safety and possible long-term effects of this approach need to be assessed in future studies.

The actuation system with linear and two rotary motors was designed using FEM simulations to meet the force and torque requirements, considering the copper losses, which are the primary source of heat to the pump system. With an average copper loss of <10 W, the ShuttlePump's power consumption is in the range of two state-of-the-art RBPs [32] and other pulsatile TAHs [33].

By using the results of the experimental hydraulic study and FEM simulations as boundary conditions for CFD simulations, hemocompatibility-related parameters of the ShuttlePump were evaluated, revealing promising results regarding blood damage, washout, and thermal behavior. The ShuttlePump shows an NIH value of 3.57 mg/100L. In context with the state-of-the-art LVAD HeartMate 3 (Abbott Inc., Illinois, United States), the numerically predicted NIH was previously reported to be 4.2 mg/100L at its best operating point of 4.5 L/min flow rate and 86 mmHg pressure head [34]. Of note, the peak shear stress observed near the in- and outlets of the pump results from high-velocity gradients. These high-velocity components, caused by backflows driven by the pressure difference between the inlets, chambers, and outlets, may be subject for future optimization of hemocompatibility by adapting the piston motion and/or dimensions.

The thrombogenic potential of the ShuttlePump was quantified through a washout study indicating 95% dye

This article has been accepted for publication in IEEE Transactions on Biomedical Engineering. This is the author's version which has not been fully edited and content may change prior to final publication. Citation information: DOI 10.1109/TBME.2023.3306888

TBME-00443-2023 9

washout in 1.42 s. Compared to the washout behavior of a generic pulsatile ventricular assist device (2.47 s for 95% washout) [27], blood remains 43.3% shorter within the ShuttlePump, indicating a superior washout behavior.

The in-silico CHT simulation results show a maximum temperature rise below 2 K caused by the power dissipated by the linear and rotary motors. This implies that the local maximum blood temperature in the gap will remain below 39°C, considering a normal blood temperature of 37°C. Although this observed local temperature rise is within requirements [19], eccentric operation of the piston may affect temperature distribution in the HB gap region and requires further investigation. In this study, we assumed a worst-case scenario with the entire power dissipated towards the blood-contacting surface. In the prototype, we will ensure uniform temperature distribution across the entire housing to avoid local heat hotspots by using thermal insulation and heat pipes/foils.

The HB gap clearance between the piston and the housing affects hemocompatibility (gap washout, heat distribution and shear stresses), bearing load capacity and bearing stability. Therefore, a trade-off needs to be found: the greater the gap clearance, the more blood can flow between the left and the right ventricular chamber. A higher gap flow is advantageous for washout and dissipation of heat. However, a larger gap clearance compromises load capacity and potentially stability of the hydrodynamic bearing. In this study, the HB design employed both analytical and numerical approaches to select bearing gap size and characterize the effective length of the bearing, which was necessary due to the difficulties posed by the side notches of the piston. A gap clearance of 140 μm was identified as an appropriate trade-off between these requirements through analytical derivations and numerical CFD simulations utilizing load capacity, volume washout, and heat dissipation. In the bearing analysis, the piston's translational motion and the axial gap flow was not considered, but may further increase bearing stiffness due to the Lomakin effect [35]. Future studies will investigate the bearing gap size and the influence of the Lomakin effect. Further a thorough in vitro evaluation of blood behavior in the bearing gap will be conducted, as the current study did not assess the hemocompatibility associated with the bearing's eccentric position. Of note, the hematocrit in the micro gap may differ from the bulk domain due to plasma skimming [36], potentially affecting cell entrainment and bearing performance.

The numerical framework to establish a stable and valid CFD simulation and assess hemocompatibility with adequate computational resources for further numerical optimization proved challenging. With the implementation of an overset mesh approach, we were able to realize the complex motion of the piston with minimal mesh deformation and with an acceptable computational power (1000 core hours per cycle). Compared to other numerical discretization techniques used in rotary piston pumps [15], the overset mesh may be more effective in accurately predicting near-wall behavior [37]. By utilizing this advanced numerical framework, future optimization of the ShuttlePump can be realized straightforwardly and effectively.

This study has potential limitations related to its in-silico and experimental character: CFD and FEM analysis were only partially validated and require further experimental validation.

Effects of inertial forces resulting from patient movement, characteristic frequencies, or undesired radial forces caused by the electromagnetic drive were not considered in the in silico studies. The power losses of the electromagnetic drive do not include core iron losses and eddy effects but only ohmic power losses. Nevertheless, the core losses are not expected to contribute considerably to the overall power losses due to the very low operational frequencies.

In our experimental setup, due to external motor overload, frequencies over 4.5 Hz with flow rates above 8 L/min could not be demonstrated but are expected to be reached with the integrated electromagnetic actuation system. Further, the negative pressures in the atria during diastole in the experimental analyses are attributable to the intrinsic limitations of the mock loop, with inertances and resistances of the stiff atrial chambers and tubes. In the clinical setting and at an adequately adjusted frequency, the atrial compliances are expected to keep the pressures in a positive range without atrial collapse.

V. CONCLUSION

This study points towards the feasibility of a new novel pumping principle for a TAH regarding implantability, pumping performance, and hemocompatibility. The pumping concept may offer a potential solution to overcome the limitations of both displacement pump and RBP concepts. The results substantiate further development toward preclinical tests in animal models to determine the TAH's safety and efficacy.

ACKNOWLEDGEMENT

REFERENCE

[1] P. Ponikowski *et al.*, "2016 ESC Guidelines for the diagnosis and treatment of acute and chronic heart failure: The Task Force for the diagnosis and treatment of acute and chronic heart failure of the European Society of Cardiology (ESC). Developed with the special contribution ," *Eur. J. Heart Fail.*, vol. 18, no. 8, pp. 891–975, 2016.

[2] J. J. Teuteberg *et al.*, "The Society of Thoracic Surgeons Intermacs 2019 Annual Report: The Changing Landscape of Devices and Indications," *Ann. Thorac. Surg.*, vol. 109, no. 3, pp. 649–660, Mar. 2020.

[3] T. D. Ryan *et al.*, "The evolving role of the total artificial heart in the management of end-stage congenital heart disease and adolescents," *ASAIO J.*, vol. 61, no. 1, pp. 8–14, Jan. 2015.

[4] S. Weinstein *et al.*, "The use of the Berlin Heart EXCOR in patients with functional single ventricle," *J. Thorac. Cardiovasc. Surg.*, vol. 147, no. 2, pp. 697–705, Feb. 2014.

[5] R. L. Kormos *et al.*, "The Society of Thoracic Surgeons Intermacs Database Annual Report: Evolving Indications, Outcomes, and Scientific Partnerships," *Ann. Thorac. Surg.*, 2019.

[6] B. Pelletier *et al.*, "System overview of the fully implantable destination therapy-ReinHeart-total artificial heart," 2014.

[7] I. L. Pieper *et al.*, "Evaluation of the novel total artificial heart Realheart in a pilot human fitting study," *Artif. Organs*, vol. 44, no. 2, pp. 174–177, Feb. 2020.

[8] A. Vis *et al.*, "The ongoing quest for the first total artificial heart as destination therapy," *Nat. Rev. Cardiol.*, vol. 19, no. 12, pp. 813–828, 2022.

This article has been accepted for publication in IEEE Transactions on Biomedical Engineering. This is the author's version which has not been fully edited and content may change prior to final publication. Citation information: DOI 10.1109/TBME.2023.3306888

TBME-00443-2023   10

[9]   K. Fukamachi *et al.*, "Generating pulsatility by pump speed modulation with continuous-flow total artificial heart in awake calves," *J. Artif. Organs*, vol. 20, no. 4, pp. 381–385, 2017.

[10]   M. Kleinheyer *et al.*, "Rapid Speed Modulation of a Rotary Total Artificial Heart Impeller," *Artif. Organs*, vol. 40, no. 9, pp. 824–833, 2016.

[11]   J. Glynn *et al.*, "The OregonHeart Total Artificial Heart: Design and Performance on a Mock Circulatory Loop," *Artif. Organs*, vol. 41, no. 10, pp. 904–910, 2017.

[12]   N. Uriel *et al.*, "Hemocompatibility-Related Outcomes in the MOMENTUM 3 Trial at 6 Months," *Circulation*, vol. 135, no. 21, pp. 2003–2012, May 2017.

[13]   J. Wappenschmidt *et al.*, "Rotary piston blood pumps: past developments and future potential of a unique pump type," *Expert Rev. Med. Devices*, vol. 13, no. 8, pp. 759–771, 2016.

[14]   C. R. Bartoli *et al.*, "A Novel Toroidal-Flow Left Ventricular Assist Device Minimizes Blood Trauma: Implications of Improved Ventricular Assist Device Hemocompatibility," *Ann. Thorac. Surg.*, vol. 107, no. 6, pp. 1761–1767, Jun. 2019.

[15]   J. Wappenschmidt *et al.*, "Fluid Dynamics in Rotary Piston Blood Pumps," *Ann. Biomed. Eng.*, vol. 45, no. 3, pp. 554–566, Mar. 2017.

[16]   A. Oliveros *et al.*, "Silicon carbide: A versatile material for biosensor applications," *Biomed. Microdevices*, vol. 15, no. 2, pp. 353–368, 2013.

[17]   M. J. Chen *et al.*, "Tailoring crystallinity for hemocompatible and durable PEEK cardiovascular implants," *Biomater. Adv.*, vol. 146, no. September 2022, p. 213288, 2023.

[18]   M. Diedrich *et al.*, "Experimental investigation of right-left flow balance concepts for a total artificial heart," *Artif. Organs*, vol. 45, no. 4, pp. 364–372, Apr. 2021.

[19]   International Organization for Standardization, "ISO 14708-1:2000 Implants for surgery — Active implantable medical devices — Part 1: General requirements for safety, marking and for information to be provided by the manufacturer," 2000.

[20]   R. V Giuffrida *et al.*, "Design and Realization of a Highly-Compact Tubular Linear Actuator for a Novel Total Artificial Hear,," TechRxiv, Preprint, https://doi.org/10.36227/techrxiv.22725674.v1, 2023.

[21]   Siemens StarCCM+ Documentation, "Mesh Quality." Siemens, 2020.

[22]   F. Boehning *et al.*, "Experimental and Analytical Performance Evaluation of Short Circular Hydrodynamic Journal Bearings Used in Rotary Blood Pumps," *Artif. Organs*, vol. 37, no. 10, pp. 913–920, Oct. 2013.

[23]   F. R. Menter, "Two-equation eddy-viscosity turbulence models for engineering applications," *AIAA J.*, vol. 32, no. 8, pp. 1598–1605, 1994.

[24]   F. W. Ocvirk, "Short-Bearing Approximation for Full Journal Bearings," 1952.

[25]   ANSYS Electronics Desktop, "ANSYS Electronics Suite 19.2; Maxwell Help; Specifying Solution Settings;" ANSYS Inc., 2022.

[26]   A. Garon and M.-I. Farinas, "Fast Three-dimensional Numerical Hemolysis Approximation," *Artif. Organs*, vol. 28, no. 11, pp. 1016–1025, 2004.

[27]   C. C. Long *et al.*, "Computation of residence time in the simulation of pulsatile ventricular assist devices," *Comput. Mech.*, vol. 54, no. 4, pp. 911–919, Oct. 2014.

[28]   M. Giersiepen *et al.*, "Estimation of shear stress-related blood damage in heart valve prostheses - in vitro comparison of 25 aortic valves," *Int. J. Artif. Organs*, vol. 13, no. 5, pp. 300–306, Apr. 1990.

[29]   D. Fiala *et al.*, "A computer model of human thermoregulation for a wide range of environmental conditions: The passive system," *J. Appl. Physiol.*, vol. 87, no. 5, pp. 1957–1972, 1999.

[30]   S. Boës *et al.*, "Hydraulic Characterization of Implantable Rotary Blood Pumps," *IEEE Trans. Biomed. Eng.*, vol. 66, no. 6, pp. 1618–1927, 2019.

[31]   S. J. Shah *et al.*, "Atrial shunt device for heart failure with preserved and mildly reduced ejection fraction (REDUCE LAP-HF II): a randomised, multicentre, blinded, sham-controlled trial," *Lancet*, vol. 399, no. 10330, pp. 1130–1140, Mar. 2022.

[32]   M. N. Belkin *et al.*, "Physiology and Clinical Utility of HeartMate Pump Parameters," *J. Card. Fail.*, vol. 28, no. 5, pp. 845–862, 2022.

[33]   M. Andriollo *et al.*, "A Review of Innovative Electromagnetic Technologies for a Totally Artificial Heart," *Appl. Sci.*, vol. 13, no. 3, 2023.

[34]   A. Escher *et al.*, "Linking Hydraulic Properties to Hemolytic Performance of Rotodynamic Blood Pumps," 2022.

[35]   R. M. Robrecht and P. F. Pelz, "The Lomakin effect at laminar flow in journal bearings – Modeling and simulation," *Tribol. Int.*, vol. 175, p. 107792, Nov. 2022.

[36]   D. Sakota *et al.*, "Plasma skimming efficiency of human blood in the spiral groove bearing of a centrifugal blood pump," *J. Artif. Organs*, vol. 24, no. 2, pp. 126–134, 2021.

[37]   A. W. Vreman, "Immersed boundary and overset grid methods assessed for Stokes flow due to an oscillating sphere," *J. Comput. Phys.*, vol. 423, Dec. 2020.